

## CONTROL OF MOBILE ROBOTS VIA BIASED WAVELET NETWORKS

**Altamiro Veríssimo da Silveira Júnior**

**Elder Moreira Hemerly**

Instituto Tecnológico de Aeronáutica ITA-IEE-IEES, Divisão de Eng. Eletrônica, Depto. de Sistemas e Controle,  
Pça. Mal. Eduardo Gomes, 50 – Vila das Acácias, 12228-900, São José dos Campos – SP

[silveira@ele.ita.br](mailto:silveira@ele.ita.br)

[hemerly@ele.ita.br](mailto:hemerly@ele.ita.br)

**Abstract** – A kinematic controller in cartesian coordinates is proposed in this paper for application in mobile robots with differential driving. Lyapunov-like analysis is employed in the control stability proof. The performance of the proposed kinematic controller is evaluated via simulation and in real time by using the Magellan-ISR mobile robot for the trajectory tracking case. Then, a Biased Wavelet Network (BWN) based controller is associated to the kinematic controller, so as to consider the effect of robot dynamic and bounded unknown disturbances. Lyapunov-like analysis is also used for establishing stable weight adaptation laws and the control system stability. Structural adaptation is used to improve the control system performance. Simulation results are presented and discussed for the dynamic control.

**Index Terms** – Wavelet networks, structural adaptation, stability proof, dynamic model, kinematic controller.

### 1.0 – INTRODUCTION

The common approach in the literature describes the mobile robot motion by the kinematic model. This model does not consider the effect of robot dynamic and external perturbations, assuming the perfect velocity tracking [1]. In [1], a kinematic controller in cartesian coordinates was proposed for solving the trajectory tracking problem. Kinematics controllers in polar coordinates were proposed in [2,3] and the convergence of the posture error was proven via Barbalat's lemma.

This work deals with both kinematic and dynamic control of mobile robots, which is a more realistic approach. The main difficulty arises when the nonlinear features, the parameters uncertainties and bounded disturbances are considered. Recently, several approaches based on neural and wavelet networks have been proposed in the literature for identification and adaptive control of nonlinear dynamic systems. In [4], the kinematic controller proposed by [1] is complemented by employing a dynamic control based on an artificial neural network (ANN), which can deal with bounded unknown disturbances, unmodeled dynamics, and external perturbations, like surface frictions. The network parameters are adapted on-line and no previous knowledge about the dynamic robot is needed, since the neural controller learns the full dynamic on-line. In [2], a dynamic control based on a biased wavelet network (BWN) with structural adaptation is associated to a kinematic controller in polar coordinates and the stability proof is discussed. Simulation results for trajectory tracking and point stabilization cases are presented. The wavelets are generated from dilations and translations of a single function  $\psi$ , which is well localized both in the space and frequency domains [5,6]. Any function in  $\mathcal{L}^2(\mathbb{R}^n)$  can be approximated with arbitrary precision by linear combinations of a wavelets set. Some advantages of wavelets over neural networks can be found in [7].

In this paper, it is proposed a kinematic controller in cartesian coordinates, which is complemented by a dynamic control based on a biased wavelet network with structural adaptation. A key step here is the use of Yamamoto [8] dynamic model for the mobile robot. The main contributions of this work are:

- Proposition of a kinematic control law in cartesian coordinates through the Lyapunov-like analysis, by proving the error convergence via Barbalat's lemma.
- Performance evaluation of the proposed kinematic controller via realistic simulation and real time implementation by employing the Magellan-ISR mobile robot.
- Stability proof of the control system based on a biased wavelet network with structural adaptation, associated to the proposed kinematic controller.
- Performance evaluation via realistic simulations of the proposed control system employing the Magellan-ISR parameters, and comparison with the kinematic-robust controller in order to show the improvement obtained by using the BWN.

This paper is structured as follows: In Section 2, a kinematic control law in cartesian coordinates is proposed and the error convergence proof is presented. In Section 3, the dynamic model developed by Yamamoto [8] is described and the controller based on a biased wavelet networks is proposed. The control system stability is proven via Lyapunov-like analysis. In Section 4, to evaluate the performance of the proposed controllers, simulations and real time implementations results are presented for the kinematic control and simulation results are also presented and discussed for the dynamic control based on a biased wavelet network. Finally in Section 5, the main conclusions are presented.

The following notation is used in this work:

$P$	Intersection of the axis of symmetry with the driving wheel axis.
$C$	Center of mass and the guidance point.
$d$	Distance from the point $C$ to the point $P$ .
$r$	Radius of wheels.
$2b$	Distance between wheels.
$c \equiv$	$r/2b$ .
$m_c$	Mobile robot mass without the motors and driving wheels.
$m_w$	Mass of each driving wheel plus its associated motor.
$m$	Mobile robot mass ( $m_c + 2m_w$ ).
$I_c$	Inertia moment of the mobile robot without the driving wheels and the motors around a vertical axis through $P$ .
$I_w$	Inertia moment of each driving wheel and the motor around the wheel axis ( $m_w(d^2 + b^2)$ ).
$I_m$	Inertia moment of each driving wheel and the motor around the wheel diameter ( $m_w r^2$ ).
$\varphi_r, \varphi_l$	Right and left wheels angles, respectively.
$v, \omega$	Linear and angular velocities of the center of mass.
$x_c, y_c, \theta$	Coordinates of point $C$ with respect to the frame $\{0, X_0, Y_0\}$ and heading angle.
$q$	Generalized coordinates, $[x_c \ y_c \ \theta \ \varphi_r \ \varphi_l]^T$ ;
$c, s$	$\cos(\theta)$ and $\sin(\theta)$ , respectively.
$diag\{.\}$	Operator that produces a diagonal matrix from a vector.
$sign\{.\}$	Signal function.
$abs(.)$	Absolute value.
$tr\{.\}$	Trace of a matrix.
$\ .\ $	Norm of vector or matrix.
$\mathbb{R}$	Real numbers set.
$\mathcal{L}^2$	Signal spaces such that $\mathcal{L}^2: \{f(.)\}: \int_0^\infty (\ f(t)\ _2)^2 dt < \infty$ , where $\ f(t)\ _2 = \sqrt{f_1^2(t) + \dots + f_n^2(t)}$ .

## 2.0 – KINEMATIC CONTROLLER

Consider in Figure 1 a mobile robot with differential driving, its local frame  $\{C, X_c, Y_c\}$  and the inertial frame  $\{0, X_0, Y_0\}$ . The robot is moving over a plane with linear velocity  $v$  and angular velocity  $\omega$ , and its position is given by the posture vector  $\mathbf{p} = [x_c \ y_c \ \theta]^T$ , containing the center of mass  $C$  coordinates and the heading angle  $\theta$ .

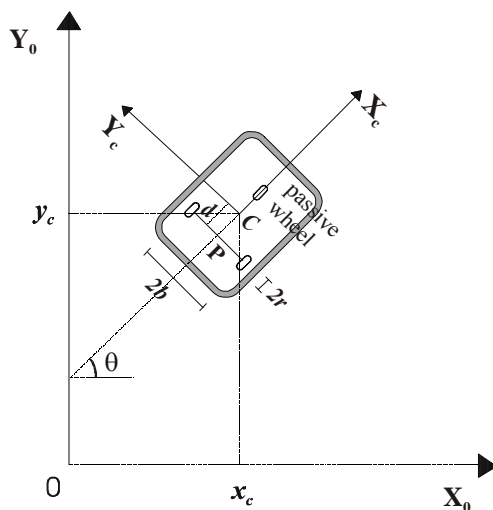


Figure 1: Mobile robot and coordinate systems

The matrix equation that describes the kinematic model in cartesian coordinates is given by

$$\begin{bmatrix} \dot{x}_c \\ \dot{y}_c \\ \dot{\theta} \end{bmatrix} = \begin{bmatrix} \cos(\theta) & -d \cdot \sin(\theta) \\ \sin(\theta) & d \cdot \cos(\theta) \\ 0 & 1 \end{bmatrix} \begin{bmatrix} v \\ \omega \end{bmatrix} \quad (1)$$

Consider now the Figure 2, where the robot C, described in Figure 1, should track the reference robot R, also described by the equation (1), moving with linear velocity  $v_r$  and angular velocity  $\omega_r$ , with posture reference  $\mathbf{p}_r = [x_r \ y_r \ \theta_r]^T$ .

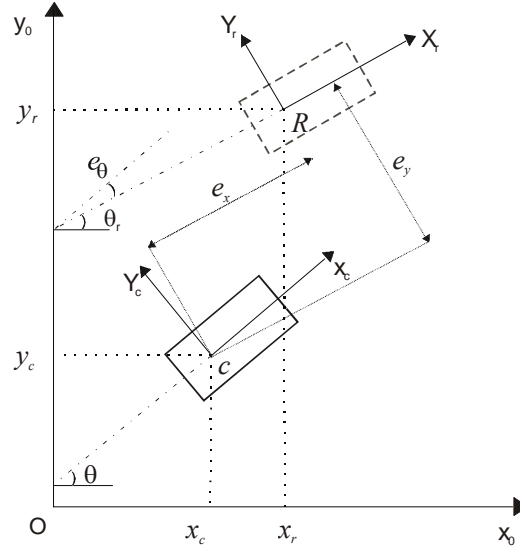


Figure 2: Mobile robot and reference robot

The posture tracking error vector  $\mathbf{e}_p$ , expressed in the basis of frame  $\{R, X_r, Y_r\}$ , is defined as

$$\mathbf{e}_p = R(\theta_r)(\mathbf{p} - \mathbf{p}_r) \quad (2)$$

or more precisely

$$\mathbf{e}_p = \begin{bmatrix} e_x \\ e_y \\ e_\theta \end{bmatrix} = \begin{bmatrix} \cos(\theta_r) & \sin(\theta_r) & 0 \\ -\sin(\theta_r) & \cos(\theta_r) & 0 \\ 0 & 0 & 1 \end{bmatrix} \begin{bmatrix} x_c - x_r \\ y_c - y_r \\ \theta - \theta_r \end{bmatrix} \quad (3)$$

where  $R(\theta_r)$  is the rotation matrix. The time derivative of the tracking error vector  $\mathbf{e}_p$  is defined as

$$\begin{bmatrix} \dot{e}_x \\ \dot{e}_y \\ \dot{e}_\theta \end{bmatrix} = \begin{bmatrix} \omega_r e_y - v_r + v \cos(e_\theta) \\ -\omega_r e_x + v \sin(e_\theta) \\ \omega - \omega_r \end{bmatrix} \quad (4)$$

Supposing a null velocity error, the kinematic control law, proposed in this work,

$$\mathbf{v}_c = \begin{bmatrix} v_c \\ \omega_c \end{bmatrix} = \begin{bmatrix} v \\ \omega \end{bmatrix} = \begin{bmatrix} v_r \cos(e_\theta) - \mathfrak{I}_x^{-1} e_x \cos(e_\theta) - \mathfrak{I}_x^{-1} e_y \sin(e_\theta) \\ \omega_r + \frac{e_x v_r}{A_\theta^2} \cdot \frac{\sin^2(e_\theta)}{e_\theta} - \mathfrak{I}_\theta^{-1} e_\theta - \frac{e_y v_r}{A_\theta^2} \cdot \cos(e_\theta) \cdot \frac{\sin(e_\theta)}{e_\theta} \end{bmatrix} \quad (5)$$

ensures stability and asymptotic convergence of posture error  $\mathbf{e}_p$  without taking into account the parameter  $d$ , where  $A_\theta$ ,  $\mathfrak{I}_x$  e  $\mathfrak{I}_\theta$  are positive constants, defined in the controller design. In order to prove this, consider the function

$$V(e_x, e_y, e_\theta) = \frac{1}{2}(e_x^2 + e_y^2) + \frac{1}{2} A_\theta^2 e_\theta^2 \quad (6)$$

which is bounded from below by zero. By differentiating the function  $V$ , and by using the equations (4) and (5), yields

$$\dot{V}(e_x, e_y, e_\theta) = -\mathfrak{I}_x^{-1} (e_x \cos(e_\theta) + e_y \sin(e_\theta))^2 - \mathfrak{I}_\theta^{-1} A_\theta^2 e_\theta^2 \quad (7)$$

which is negative semi-definite. From equations (6) and (7), we conclude that  $e_x$ ,  $e_y$  and  $e_\theta$  are bounded. By differentiating the equation (7), we know that  $\ddot{V}(e_x, e_y, e_\theta)$  is also bounded. By using the Barbalat's lemma, it follows that  $\dot{V}(e_x, e_y, e_\theta)$  is uniformly continuous, thereby converging to zero. Then,  $e_x$  and  $e_\theta$  converge to zero. From equation (4), we verify that  $e_y$  converges to a constant. By applying the Barbalat's lemma in equation (4), it follows that  $\ddot{e}_\theta$  is bounded and this way  $\dot{e}_\theta \rightarrow 0$ .

By returning to equation (5) and since  $\omega \rightarrow \omega_r$ , we can verify that  $e_y \rightarrow 0$ , concluding the proof. Figure 3 shows the diagram of the kinematic controller in cartesian coordinates.

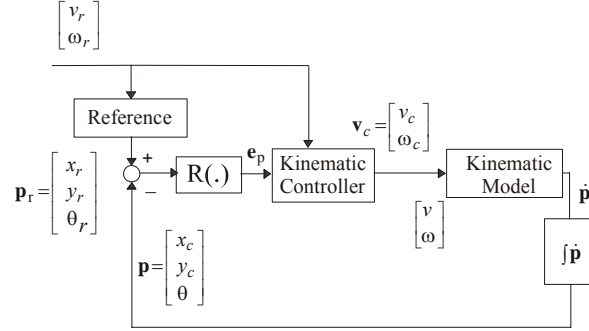


Figure 3: Diagram of the kinematic controller

### 3.0 – DYNAMIC CONTROLLER

#### 3.1. Dynamic Model

For modeling the dynamic features of the mobile robot, the Lagrange method is employed, as in Yamamoto [8]. The dynamic equation of the mobile robot can be written as

$$M(\mathbf{q})\ddot{\mathbf{q}} + V_m(\mathbf{q}, \dot{\mathbf{q}}) + N(\dot{\mathbf{q}}) + \tau_d = E(\mathbf{q})\tau - A^T(\mathbf{q})\lambda \quad (8)$$

where  $M(\mathbf{q}) \in \mathfrak{R}^{n \times n}$  is the inertia matrix, which is symmetric and positive definite,  $V_m(\mathbf{q}, \dot{\mathbf{q}}) \in \mathfrak{R}^{n \times 1}$  is the centripetal and Coriolis matrix,  $N(\dot{\mathbf{q}}) \in \mathfrak{R}^{n \times 1}$  is the surface friction vector,  $\tau_d \in \mathfrak{R}^{n \times 1}$  represents bounded unknown disturbances including unmodeled dynamics,  $E(\mathbf{q}) \in \mathfrak{R}^{n \times 2}$  is the input transformation matrix,  $\tau \in \mathfrak{R}^{2 \times 1}$  is the control signal,  $A(\mathbf{q}) \in \mathfrak{R}^{m \times n}$  is the matrix containing the movement restrictions and  $\lambda \in \mathfrak{R}^{m \times 1}$  is the Lagrange multiplier ( $n=5$  and  $m=3$ ).

The matrices  $M(\mathbf{q})$ ,  $V_m(\mathbf{q}, \dot{\mathbf{q}})$ ,  $E(\mathbf{q})$  and  $A(\mathbf{q})$  can be found in [8],

$$M(\mathbf{q}) = \begin{bmatrix} m & 0 & -m_c ds & 0 & 0 \\ 0 & m & m_c dc & 0 & 0 \\ -m_c ds & m_c dc & I & 0 & 0 \\ 0 & 0 & 0 & I_\omega & 0 \\ 0 & 0 & 0 & 0 & I_\omega \end{bmatrix}, \quad V_m(\mathbf{q}, \dot{\mathbf{q}})\dot{\mathbf{q}} = \begin{bmatrix} -m_c d \dot{\theta}^2 c \\ -m_c d \dot{\theta}^2 s \\ 0 \\ 0 \\ 0 \end{bmatrix}, \quad E(\mathbf{q}) = \begin{bmatrix} 0 & 0 \\ 0 & 0 \\ 0 & 0 \\ 1 & 0 \\ 0 & 1 \end{bmatrix}$$

$$A(\mathbf{q}) = \begin{bmatrix} -s & c & -d & 0 & 0 \\ -c & -s & -R & r & 0 \\ -c & -s & -R & 0 & r \end{bmatrix} \quad (9)$$

The kinematic model in this coordinate system is described by

$$\dot{\mathbf{q}} = S(\mathbf{q})\eta \quad (10)$$

where  $\eta = [\dot{\phi}_r \ \dot{\phi}_l]^T$  represents the angular velocity vector, for the right and left wheels, respectively, and  $S(\mathbf{q})$  is given by

$$S(\mathbf{q}) = \begin{bmatrix} c(Rc-ds) & c(Rc+ds) \\ c(Rs+dc) & c(Rs-dc) \\ c & -c \\ 1 & 0 \\ 0 & 1 \end{bmatrix} \quad (11)$$

By using equation (10), we can rewrite equation (8) as

$$\bar{M} \dot{\eta} + \bar{V}_m \eta + \bar{N}(\eta) + \bar{\tau}_d = \bar{\tau} \quad (12)$$

where  $\bar{M}$ ,  $\bar{V}_m$ ,  $\bar{N}(\eta)$ ,  $\bar{\tau}_d$  and  $\bar{\tau}$  are defined in a similar way to the matrices  $M(\mathbf{q})$ ,  $V_m(\mathbf{q}, \dot{\mathbf{q}})$ ,  $N(\dot{\mathbf{q}})$ ,  $\tau_d$  and  $\tau$ , respectively [4]. The relationship between the wheels and the mass of center velocity is given by

$$\begin{bmatrix} \dot{\phi}_r \\ \dot{\phi}_l \end{bmatrix} = \Sigma \begin{bmatrix} v \\ \omega \end{bmatrix} \quad (13)$$

where  $\Sigma = \begin{bmatrix} \frac{l}{r} & \frac{b}{r} \\ \frac{l}{r} & -\frac{b}{r} \end{bmatrix}$ .

**Definition 1:** Let  $\mathbf{v}_c$  be the control velocity and  $\eta$  the robot velocity. Then, the velocity error in dynamic model is  $\mathbf{e}_c = \Sigma \mathbf{v}_c - \eta$  and the velocity error in kinematic model is  $\mathbf{e}_{ck} = \mathbf{v}_c - \Sigma^{-1} \eta$ . The relationship between the errors is given by

$$\mathbf{e}_c = \Sigma \mathbf{e}_{ck} \quad (14)$$

with  $\mathbf{e}_{ck} = [e_v \ e_\omega]^T$  defined as

$$\mathbf{e}_{ck} = \begin{bmatrix} e_v \\ e_\omega \end{bmatrix} = \begin{bmatrix} v_c - v \\ \omega_c - \omega \end{bmatrix} \quad (15)$$

The dynamic equation (12) can then be written as a  $\mathbf{e}_c$  function [4],

$$\bar{M} \dot{\mathbf{e}}_c = -\bar{V}_m \mathbf{e}_c - \bar{\tau} + f(x) + \bar{\tau}_d \quad (16)$$

where  $\bar{\tau}_d$  represents bounded disturbances including unstructured uncertainties and  $f(x) = \bar{M} \Sigma \dot{\mathbf{v}}_c + \bar{V}_m \Sigma \mathbf{v}_c + \bar{N}(\eta)$  is a nonlinear function, containing robot dynamic, trajectory information, surfaces friction and other parameters which are difficult to estimate. The vector  $x$  used to estimate the function  $f(x)$  is given by  $[1 \ \eta^T \ \Sigma \mathbf{v}_c^T \ \Sigma \dot{\mathbf{v}}_c^T]^T$ , composed by the velocity signal, control signal and its derivative.

### 3.2. Wavelets

A wavelet is a function that can be shifted along the independent axis (translation) and rescaled, such that appears squashed and expanded along the independent axis (dilation). A wavelet set  $\Lambda$  can be generated from dilations and translations of a single function  $\psi$ , defined as wavelet mother, in the following form

$$\Lambda \triangleq \{ \psi^{a,b} \in L^2(\mathbf{R}); \psi^{a,b}(z) = |a|^{-\frac{1}{2}} \psi\left(\frac{z-b}{a}\right), a \in \mathbf{R}^*, b \in \mathbf{R}; \} \quad (17)$$

where  $a$  corresponds to the dilation parameter,  $b$  is the translation parameter and  $z$  represents a real variable. The wavelet  $\psi$  is an oscillatory function with zero mean, such that  $\psi \in L^2(\mathbf{R})$ . Combinations of wavelets can be used to generate a domain over which data is to be modeled, similar to the way that radial basis functions (RBF) are used in the neural networks. Unlike neural networks, wavelets should satisfy certain admissibility condition, which forces the zero mean restriction, implying that

$$\int_{-\infty}^{\infty} \frac{|\tilde{\psi}(\varpi)|^2}{|\varpi|} d\varpi < \infty \quad (18)$$

where  $\tilde{\psi}(\varpi)$  is the Fourier transform of the wavelet  $\psi$  and  $\varpi \in \mathbb{R}$ . The continuous wavelet transform of a function  $f$  is given by

$$(T^{wav}f)(a,b) = \langle f, \psi^{a,b} \rangle = \int_{-\infty}^{\infty} f(z) \psi^{a,b}(z) dz = |a|^{-\frac{1}{2}} \int_{-\infty}^{\infty} f(z) \psi\left(\frac{z-b}{a}\right) dz \quad (19)$$

and the inverse wavelet transform can be obtained by

$$f = C_{\psi}^{-1} \int_{-\infty}^{\infty} \int_{-\infty}^{\infty} a^{-2} (T^{wav}f)(a,b) \psi^{a,b} da db \quad (20)$$

where

$$C_{\psi} = 2\pi \int_{-\infty}^{\infty} \frac{|\tilde{\psi}(\varpi)|^2}{|\varpi|} d\varpi \quad (21)$$

A key property of wavelets in the control and estimation analysis is that they have high resolution in both space and spatial frequency domains, providing a framework for resolving data at varying levels of detail, which is defined as multi-resolution analysis. In this work, tuning rules are developed for adjust the dilations, translations and output parameters on-line as well as the wavelons number that are used in the algorithms.

### 3.3. Biased Wavelet Network

Consider a feedforward wavelet networks with two layers,  $n$  inputs,  $m$  outputs, wavelet and radial activation functions in the hidden layer and linear activation function in the output layer, described by

$$y_i = \sum_{j=1}^{N_h} [\omega_{ij} \psi(\sum_{k=1}^n v_{jk} x_k + \theta_{vj} - d_j) + \theta_{wi}] + \sum_{j=1}^{N_h} [u_{ij} \zeta(\sum_{k=1}^n v_{jk} x_k + \theta_{vj} - d_j) + \theta_{ui}] \quad (22)$$

where  $N_h$  represents the number of wavelons in the hidden layer,  $x_k$  a component of the input vector network,  $\psi(\cdot)$  the wavelet activation function,  $\zeta(\cdot)$  the bias activation function,  $d_j$  the translation parameter,  $v_{jk}$  the dilation parameter,  $\omega_{ij}$  the wavelets parameters in the output layer,  $u_{ij}$  the bias parameters in the output layer. The terms  $\theta_{vj}$ ,  $\theta_{wi}$  and  $\theta_{ui}$  correspond to the *offsets* of hidden and outputs layers respectively (wavelet and bias).

The matrix notation of equation (22) is given by

$$Y = W\psi(Vx - D) + U_{\zeta}(Vx - D) \quad (23)$$

which is different from conventional parameterization due to the second term. The bias term is able to represent more precisely the low frequency features of the function and it also enables estimation of functions with nonzero mean. Basically, it has a more flexible structure than the conventional parameterization.

The wavelets are well localized both in space and frequency domains and can approximate any function  $f(x) \in \mathcal{L}^2(\mathbb{R}^n)$  with arbitrary precision. Then, a nonlinear function  $f(x) \in \mathcal{L}^2(\mathbb{R}^n)$  can be written as

$$f(x) = W\psi(Vx - D) + U_{\zeta}(Vx - D) \quad (24)$$

and an estimate of  $f(x)$  can be obtained by

$$\hat{f}(x) = \hat{W}\psi(\hat{V}x - \hat{D}) + \hat{U}_{\zeta}(\hat{V}x - \hat{D}) \quad (25)$$

where  $\hat{f}(x)$  is the BWN output,  $\hat{W}, \hat{V}, \hat{U}$  and  $\hat{D}$  are the estimate of the matrixes  $W, V, U$  and  $D$ , respectively, representing the ideal weights of the networks. Therefore, there is a reconstruction error

$$\varepsilon = f(x) - \hat{f}(x) \quad (26)$$

Unlike the wavelets  $\psi(\cdot)$ , the bias term should be a nonzero mean function in order to reproduce low-frequency features more easily and at the same time work as a scaling function, reducing the number of multi-resolution levels required in the approximation process. Good results were obtained in [9] for data compression, by using the biased wavelet network, which motivates its application in other domains.

According to [9], a prospective bias function should satisfy the following conditions:

- $\zeta \in L^2(\mathbb{R})$ ;
- $\zeta(0) \neq 0$ ;
- $|\zeta(z)|$  rapidly decreases to zero when  $|z| \rightarrow +\infty$ ;
- $|\zeta(\varpi)|$  rapidly decreases to zero when  $|\varpi| \rightarrow +\infty$ ;
- 

**Definition 2:** Consider  $\hat{Z} = \text{diag}\{\hat{W}^T, \hat{U}^T, \hat{V}, \hat{D}\}$  as a weight matrix of the BWN, given by

$$\hat{Z} = \begin{bmatrix} \hat{W}^T & 0 & 0 & 0 \\ 0 & \hat{U}^T & 0 & 0 \\ 0 & 0 & \hat{V} & 0 \\ 0 & 0 & 0 & \hat{D} \end{bmatrix} \quad (27)$$

The matrices  $\tilde{V} = V - \hat{V}$ ,  $\tilde{W} = W - \hat{W}$ ,  $\tilde{U} = U - \hat{U}$  and  $\tilde{D} = D - \hat{D}$  are defined as the estimation error of weight matrices  $V, W, U$  and  $D$ , respectively. In this work, the employed mother wavelet is  $\psi(z) = \sin(1.5z) \cdot \exp(-\frac{z^2}{2})$  where  $z = \hat{V}x - \hat{D}$  corresponds to the hidden layer input vector. The bias function was chosen as  $\zeta(z) = \exp(-\frac{z^2}{2})$ , which provides the best trade-off between space and frequency resolution [9]. Figure 4 illustrates the connections in the hidden layer.

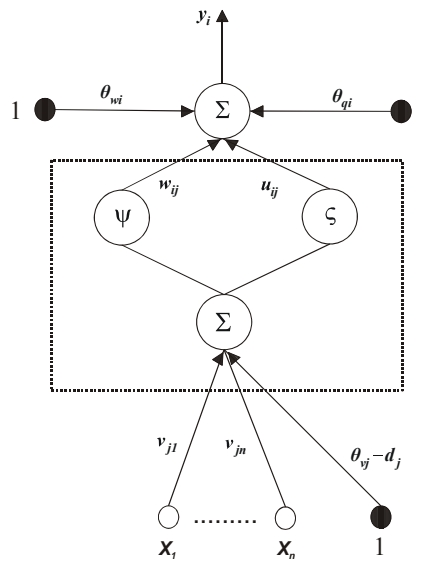


Figure 4: Wavelon connections in the hidden layer

### 3.4. Structural Adaptation

A structural adaptation algorithm for wavelet networks was proposed in [10], which was used to control a robotic manipulator. However, in [10] only the parameters in the output layer are allowed to adapt. In this work, the dilations and translations

parameters will also adapted on-line as well as the wavelet structure. The structural adaptation adjusts the number of nodes in the hidden layer in real time, discharging the wavelons that are redundant in the estimation process and introducing new wavelons in the structure, when the network is not able to estimate the function appropriately.

The wavelons in the hidden layer can be classified into three sets, according to the output layer coefficients. At time  $t$ , if exists at least one node in the  $\mathcal{L}^+$  set, then a new wavelon should be introduce into the network. The nodes that belong to the  $\mathcal{L}^-$  set should be eliminated from the network and the nodes that belong to the  $\mathcal{L}^0$  set do not affect the adaptation process, remaining into the structure. The algorithm only introduces or excludes one node to the network by iteration. The sets are defined according to the following rules

$$\begin{aligned} \mathcal{L}^+ : \forall j \quad & \text{if } \|W_j\|_t - \|W_j\|_{t-\Delta t} > \mu_1 \\ \mathcal{L}^0 : \forall j \quad & \text{if } -\mu_2 \leq \|W_j\|_t - \|W_j\|_{t-\Delta t} \leq \mu_1 \\ \mathcal{L}^- : \forall j \quad & \text{if } \|W_j\|_t - \|W_j\|_{t-\Delta t} < -\mu_2 \end{aligned}$$

where  $\|W_j\|_t$  is the weight norm associated to the wavelon  $j$  in the instant  $t$ ,  $\Delta t$  corresponds to the sampling time,  $\mu_1$  and  $\mu_2$  are positive constants, adjusted according to the dynamic system providing better controller performance. The structural adaptation process is defined according to the following rules:

- Select a node in the  $\mathcal{L}^-$  set to be removed for an each instant  $t$ .
- If  $\mathcal{N}(\mathcal{L}^+) \neq 0$ , introduce a node in the structure, where  $\mathcal{N}(\cdot)$  is the number of elements set.
- The number of nodes  $N_h$  has a lower bound equal to one and a upper bound equal to  $N_{hmax}$ .

### 3.5. Dynamic Control via BWN

Considering the robot dynamic, uncertainties in modeling and external perturbations, such as surface friction, a dynamic control law based on [4] is used,

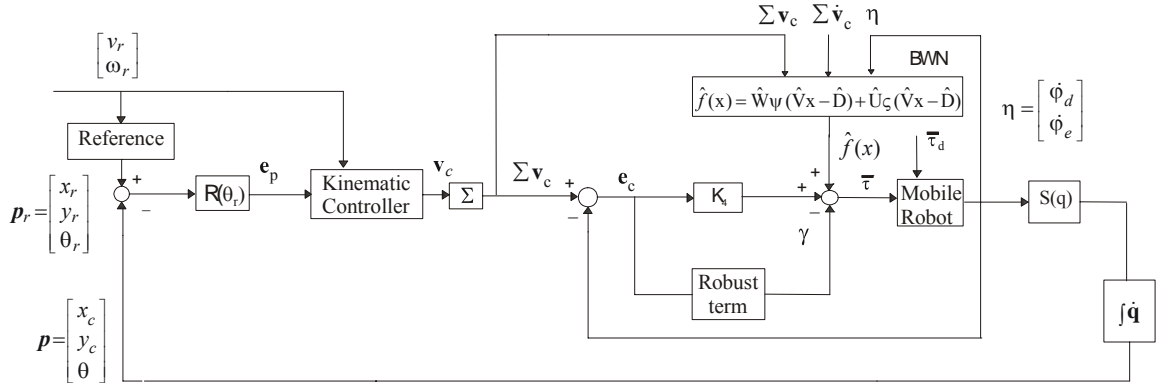


Figure 5: Dynamic control via BWN

$$\bar{\tau} = \hat{f}(x) + k_4 I e_c - \gamma \quad (28)$$

where  $k_4$  is a positive constant,  $\hat{f}(x)$  the BWN output and  $\gamma$  the robust term, given by

$$\gamma = -k_z (\|\hat{Z}\|_F + Z_M) e_c - e_c \quad (29)$$

which  $k_z$  is a positive constant,  $\|\hat{Z}\|_F$  is the Frobenius norm of  $\hat{Z}$  and  $Z_M$  is the Frobenius norm upper bound of matrix  $Z$ . By replacing equation (28) into equation (16) and by using the Taylor series expansion, like in [4] we get

$$\bar{M} \dot{e}_c = -(k_4 I + \bar{V}_m) e_c + \hat{W} \hat{\Psi} (\tilde{V}x - \tilde{D}) + \tilde{W} (\hat{\psi} - \hat{\Psi} (\hat{V}x - \hat{D})) + \hat{U} \hat{\Phi} (\tilde{V}x - \tilde{D}) + \tilde{U} (\hat{\zeta} - \hat{\Phi} (\hat{V}x - \hat{D})) + \gamma + \delta \quad (30)$$

where the disturbance term  $\delta$  is defined as

$$\delta = (\varepsilon + \bar{\tau}_d) + \tilde{W} \hat{\Psi} (\tilde{V}x - \tilde{D}) + \tilde{W} O_1 (\tilde{V}x - \tilde{D}) + \tilde{U} \hat{\Phi} (\tilde{V}x - \tilde{D}) + \tilde{U} O_2 (\tilde{V}x - \tilde{D}) \quad (31)$$



with  $O_1(\tilde{V}x - \tilde{D})$  and  $O_2(\tilde{V}x - \tilde{D})$  corresponding to higher-order terms,  $\hat{\Psi}$  and  $\hat{\Phi}$  stand for the derivatives of the wavelet and bias activation functions, respectively. The  $\delta$  norm is bounded by

$$\|\delta\| \leq C_0 + C_1 \|\tilde{Z}\|_F + C_2 \|\tilde{Z}\|_F \|\mathbf{e}_c\| \quad (32)$$

where  $C_i$ ,  $i=0,1,2$  are positive constants.

**Theorem** : Consider the control system represented in figure 5, described by equations (10) and (16), and the following assumptions:

- The kinematic and dynamic controllers given by (5) and (28), respectively.
- The BWN adaptation law, given by the tuning rules,

$$\begin{aligned} \dot{\hat{W}}_j^T &= F_j \hat{\Psi} \mathbf{e}_c^T - F_j \hat{\Psi} (\hat{V}_j x - \hat{D}_j) \mathbf{e}_c^T - k F_j \|\mathbf{e}_c\| \hat{W}_j^T \\ \dot{\hat{V}}_j &= G_j \hat{\Psi}^T \hat{W}_j^T \mathbf{e}_c x^T + G_j \hat{\Phi} U_j^T \mathbf{e}_c x^T - k G_j \|\mathbf{e}_c\| \hat{V}_j \\ \dot{\hat{D}}_j &= -H_j \hat{\Psi}^T \hat{W}_j^T \mathbf{e}_c - H_j \hat{\Phi} U_j^T \mathbf{e}_c - k H_j \|\mathbf{e}_c\| \hat{D}_j \\ \dot{\hat{U}}_j^T &= J_j \hat{\xi} \mathbf{e}_c^T - J_j \hat{\Phi} (\hat{V}_j x - \hat{D}_j) \mathbf{e}_c^T - k J_j \|\mathbf{e}_c\| \hat{U}_j^T \end{aligned} \quad \text{if } j \in \mathbb{L}^+, \mathbb{L}^0 \quad (33)$$

$$\begin{aligned} \dot{\hat{W}}_j^T &= F_j \hat{\Psi} \mathbf{e}_c^T - F_j \hat{\Psi} (\hat{V}_j x - \hat{D}_j) \mathbf{e}_c^T - F_j \frac{\text{sign}(\hat{W}_j)}{\mathcal{N}(\mathbb{L}^-)} \\ \dot{\hat{V}}_j &= G_j \hat{\Psi}^T \hat{W}_j^T \mathbf{e}_c x^T + G_j \hat{\Phi} U_j^T \mathbf{e}_c x^T \\ \dot{\hat{D}}_j &= -H_j \hat{\Psi}^T \hat{W}_j^T \mathbf{e}_c - H_j \hat{\Phi} U_j^T \mathbf{e}_c \\ \dot{\hat{U}}_j^T &= J_j \hat{\xi} \mathbf{e}_c^T - J_j \hat{\Phi} (\hat{V}_j x - \hat{D}_j) \mathbf{e}_c^T \end{aligned} \quad \text{if } j \in \mathbb{L}^- \quad (34)$$

where  $F, G, J$  and  $H$  are positive definite matrices and  $k$ , a positive constant defined in the design.

Then, the posture error  $\mathbf{e}_p$ , the velocity error  $\mathbf{e}_c$ , the BWN weight estimation error ( $\tilde{Z}$ ) are uniformly ultimately bounded (UUB).

**Proof** : Consider the function  $V$

$$V(\mathbf{e}_p, \mathbf{e}_c, \tilde{Z}) = \frac{1}{2} (e_x^2 + e_y^2) + \frac{1}{2} A_\theta^2 e_\theta^2 + V_1 \quad (35)$$

Where

$$V_1 = \frac{1}{2} [\mathbf{e}_c^T \bar{M} \mathbf{e}_c + \text{tr}\{\tilde{W} F^{-1} \tilde{W}^T\} + \text{tr}\{\tilde{V}^T G^{-1} \tilde{V}\} + \text{tr}\{\tilde{U} J^{-1} \tilde{U}^T\} + \text{tr}\{\tilde{D}^T H^{-1} \tilde{D}\}] \quad (36)$$

Differentiating  $V(\mathbf{e}_p, \mathbf{e}_c, \tilde{Z})$ , we get

$$\dot{V}(e_x, e_y, e_\theta) = v.(e_x \cos(e_\theta) + e_y \sin(e_\theta)) - e_x v_r + A_\theta^2 e_\theta (\omega - \omega_r) + \dot{V}_1 \quad (37)$$

By using the equations (5), (14), (15), (30), (33), (34) and the skew symmetry property of  $\dot{\bar{M}} - 2\bar{V}_m$  [4], yields

$$\begin{aligned} \dot{V} \leq & \left(\frac{r^2}{8} - \mathfrak{I}_x^{-1}\right)(e_x \cos(e_\theta) + e_y \sin(e_\theta))^2 + \left(\frac{r^2}{8R^2} A_\theta^2 - \mathfrak{I}_\theta^{-1}\right) A_\theta^2 e_\theta^2 - \left(\frac{\sqrt{2}}{r} e_v + \frac{r}{2\sqrt{2}}(e_y \sin(e_\theta) + e_x \cos(e_\theta))\right)^2 \\ & - \left(\frac{\sqrt{2}}{r} R e_\omega + \frac{r}{2\sqrt{2}R} (A_\theta^2 e_\theta)\right)^2 - \mathbf{e}_c^T k_4 \mathbf{e}_c + k \|\mathbf{e}_c\| \operatorname{tr}\{\tilde{W}\hat{W}^T\}_{j \in L_0, L_+} + k \|\mathbf{e}_c\| \operatorname{tr}\{\tilde{V}^T \hat{V}\}_{j \in L_0, L_+} \\ & + k \|\mathbf{e}_c\| \operatorname{tr}\{\tilde{D}^T \hat{D}\}_{j \in L_0, L_+} + k \|\mathbf{e}_c\| \operatorname{tr}\{\tilde{U}\hat{U}^T\}_{j \in L_0, L_+} + \operatorname{tr}\left\{\frac{\tilde{W}\operatorname{sign}(\hat{W}^T)}{\mathcal{N}(L^-)}\right\}_{j \in L^-} + \mathbf{e}_c^T (\delta + \gamma) \end{aligned} \quad (38)$$

To make the first and the second terms negative, the following inequalities should hold,

$$\mathfrak{I}_x < \frac{8}{r^2} \quad \text{and} \quad \mathfrak{I}_\theta < \frac{8R^2}{r^2 A_\theta^2} \quad (39)$$

By using a procedure similar to [7], it follows that  $\tilde{W}\operatorname{sign}(\hat{W}^T) = \tilde{W}\operatorname{sign}(W - \tilde{W}_j^T) = \tilde{W}\operatorname{sign}(-\tilde{W}_j^T) = -\operatorname{abs}(\tilde{W}_j)$ , because  $W=0$  for  $j \in L^-$ . By replacing equations (29) and (32) into (38), considering  $k_2 > C_2$  and knowing that

$$\operatorname{tr}\{\tilde{Z}^T (Z - \tilde{Z})\} = \langle \tilde{Z}, Z \rangle_F - \|\tilde{Z}\|_F^2 \leq \|\tilde{Z}\|_F \|Z\|_F - \|\tilde{Z}\|_F^2 \quad (40)$$

Defining now  $C_3 = \frac{1}{2} \cdot (Z_M + \frac{C_1}{k})$ , it follows that

$$\dot{V} \leq -\|\mathbf{e}_c\| \cdot [k_{4min} \|\mathbf{e}_c\| + k(\|\tilde{Z}_{j \in L_+, L_0}\|_F - C_3)^2 - C_0 - kC_3^2] \quad (41)$$

To make the expression between brackets positive, we need

$$\|\mathbf{e}_c\| > \frac{kC_3^2 + C_0}{k_{4min}} \equiv b_c \quad \text{or} \quad \|\tilde{Z}\|_F > C_3 + \sqrt{C_3^2 + \frac{C_0}{k}} \equiv b_z \quad (42)$$

Figure 6 shows the convergence region.

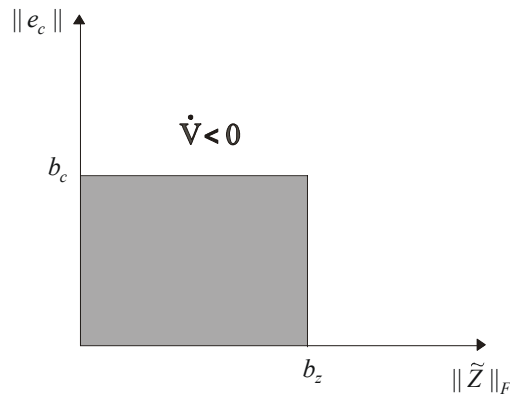


Figure 6: Convergence region

Hence,  $\dot{V}$  is negative outside a compact set and this demonstrates that  $\|\mathbf{e}_c\|$  and  $\|\tilde{Z}\|$  are UUB, as required by the theorem. Equation (42) represents the worst case we can have since  $\dot{V}$  can be also negative inside the indicated compact set. The weights associated to the  $L^-$  set are bounded by definition, thence do not affect the stability proof. It should be stressed that the stability proof is semi-global, in the sense that the state vector  $x$  required in the wavelet network to estimate the function  $f(x)$  should belong to a compact set, according to the universal approximation theorem [11].

#### 4.0 – SIMULATION RESULTS AND REAL TIME IMPLEMENTATIONS

To illustrate the theoretical results presented in Sections 2 and 3, the proposed kinematic controller performance is evaluated via simulation and in real time by using the Magellan-ISR mobile robot for the trajectory tracking case. The performance of the proposed dynamic control is also evaluated by simulation. The simulations were performed in MATLAB software, version 5.3, and the real time applications were implemented in MOBILITY software, version 1.0 [12]. The distance between the guidance point and symmetry point was calculated experimentally and results in  $d = 0.02$  m. The Magellan-ISR robot includes two independents driver motors at each conventional fixed wheels, placed on the same axis, and one conventional off-centered free wheel [12]. Figure 7 shows the Magellan-ISR mobile robot.

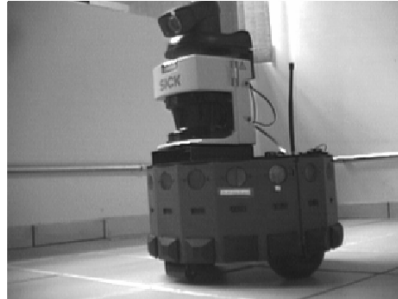


Figure 7: Magellan-ISR mobile robot

For the kinematic controller, the same conditions were considered in simulation and real time application, to establish a coherent comparison. The Euler method was employed for equation integration with time step  $T=0.1$  s. Several integration methods were tested including Runge-Kutta, but with only marginal improvement. The norms of both linear and angular velocity control signals were limited respectively in  $|v_c| \leq 1.0$  m/s and  $|\omega_c| \leq 2.0$  rad/s. To avoid prohibitive control effort in transient period, saturation in control signals was used with time derivative equal to  $0.3$  m/s<sup>2</sup> for  $v_c$  and  $0.5$  rad/s<sup>2</sup> for  $\omega_c$ . In simulation algorithm, a white noise ( $\tau_v$ ) modeled by a gaussian distribution with zero mean and a variance ( $N(0; \sigma^2)$ ) was introduced in velocity signal ( $v$  and  $\omega$ ) to reproduce the conditions of the real time case and verify the robustness of the control law.

For the trajectory tracking case, a circular reference trajectory was considered, with  $v_r = 0.4$  m/s,  $\omega_r = 0.4$  rad/s. A velocity noise  $\tau_v$  was defined with a variance equal to  $2.5 \times 10^{-5}$  and the following kinematic controller gains:  $A_\theta = 0.4$ ,  $\mathfrak{I}_x = 1.0$  and  $\mathfrak{I}_\theta = 1.0$ . The initial reference trajectory posture is given by  $\mathbf{p}_r = (1.0, 0, \pi/2)$  and the robot starts with initial condition  $\mathbf{p} = (0, 0, 0)$ . The results obtained for the simulation case are shown in figures 8–11.

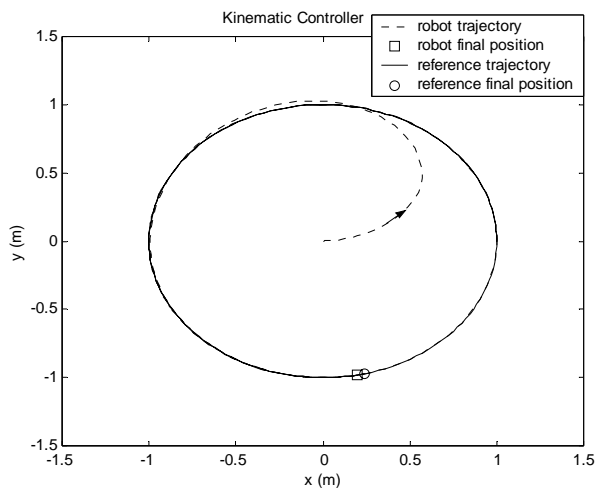


Figure 8: Robot and reference trajectory

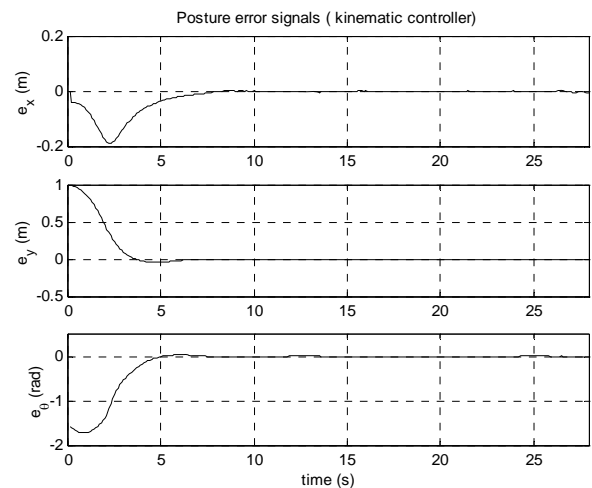


Figure 9: Posture error signals

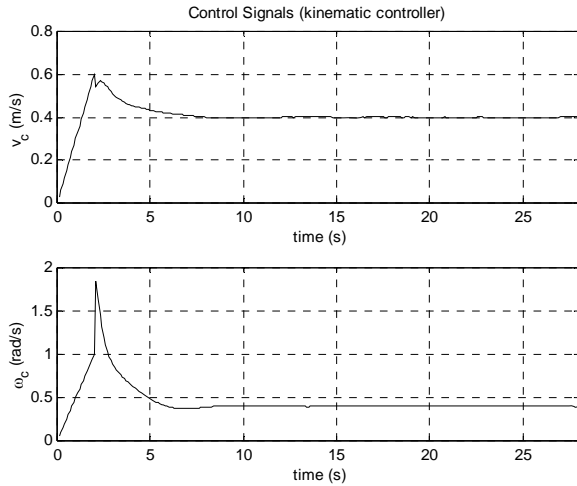


Figure 10: Control signals ( $v_c$  and  $\omega_c$ )

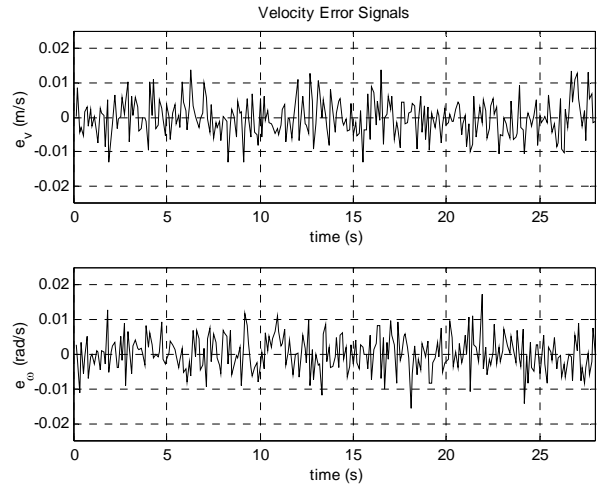


Figure 11: Velocity error signals ( $e_v$  and  $e_\omega$ )

From figures 8 and 9, we conclude that the kinematic controller provided the asymptotic convergence of the posture error, as expected, and it was sufficiently robust to compensate the velocity error, which is considered null in the stability proof.

We now consider the experimental case. The kinematic controller gains was selected as:  $A_\theta=0.4$ ,  $\mathfrak{I}_x=1.0$  and  $\mathfrak{I}_\theta=1.0$ . The robot velocities are calculated by differentiating the position information provided by odometer. The results are presented in figures 12–15.

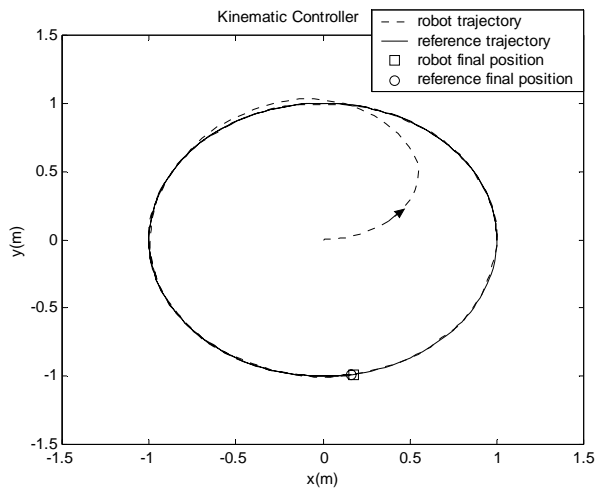


Figure 12: Robot and reference trajectory

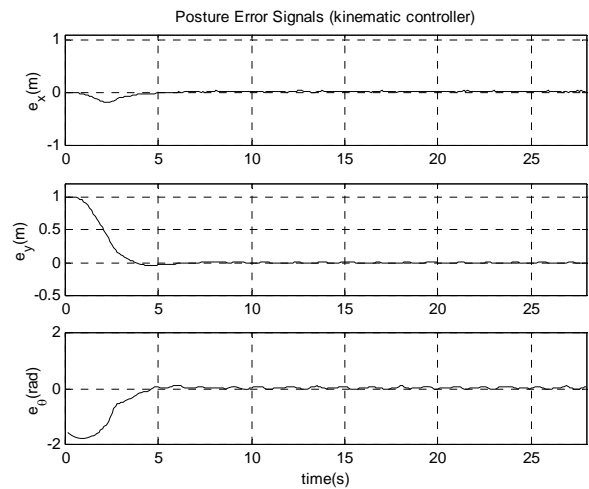


Figure 13: Posture error signals

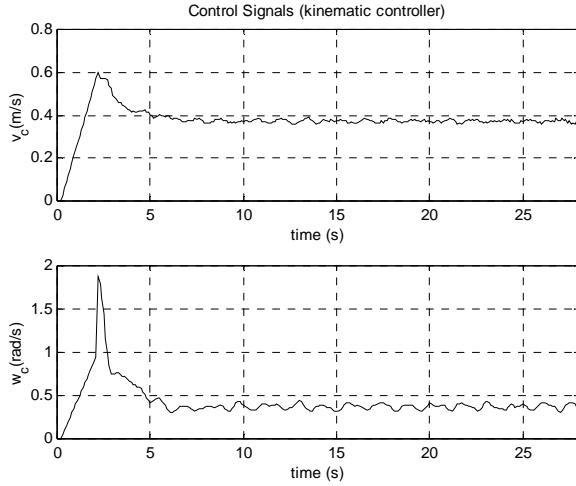


Figure 14: Control signals ( $v_c$  and  $\omega_c$ )

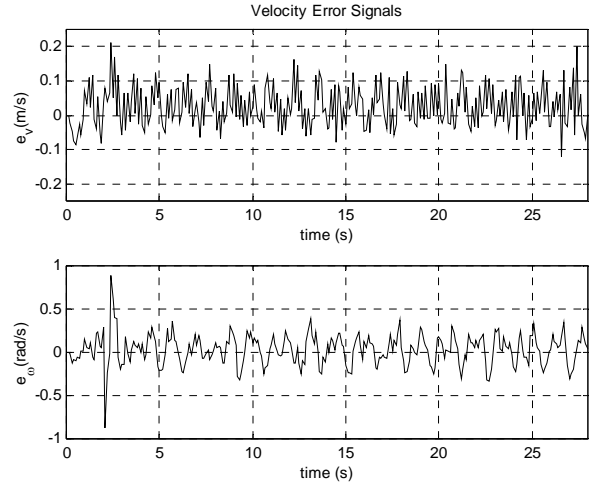


Figure 15: Velocity error signals ( $e_v$  and  $e_\omega$ )

From figures 8–15 we conclude that the experimental results were compatible with those obtained via simulation. The kinematic controller was able to ensure the posture error convergence, presenting at the same time sufficient robustness to compensate the velocity error, which kept bounded and sufficiently small during the real time application, thereby not affecting the controller performance.

Consider now the dynamic controller based on a biased wavelet network, described in Section 3, associated to the kinematic controller. The Magellan-ISR mobile robot parameters and disturbances are:

- $m_c = 22.9644$  kg,  $m_w = 0.5678$  kg,  $I_c = 0.4732$  kg.m<sup>2</sup>,  $I_w = 0.0198$  kg.m<sup>2</sup>,  $I_m = 0.0018$  kg.m<sup>2</sup>,  $d = 0.02$ m,  $r = 0.057$ m,  $b = 0.18$ m,  $\|\bar{N}(\eta)\| \leq 4.0$  N and  $\bar{\tau}_d = N(0;0.5)$ .<sup>a</sup>

The kinematic and dynamic controllers gains were chosen as:

- $A_\theta = 0.5$ ,  $\mathfrak{I}_x = 0.5$ ,  $\mathfrak{I}_\theta = 0.5$ ,  $k_4 = 0.01$ ,  $k_z = 10^{-4}$ ,  $Z_M = 10$ ,  $F = G = H = J = 0.2 \mathbf{I}_{N_h \times N_h}$  and  $k = 1.7$ .

The networks parameters for structural adaptation are selected as:

- $\mu_1 = 0.009$ ,  $\mu_2 = 0.01$  and  $N_{hmax} = 25$ .

The sampling time  $T = 0.01$  s was used in the simulations. The kinematics control signals were bounded by  $|v_c| \leq 2.5$  m/s and  $|\omega_c| \leq 3\pi/2$  rad/s, which are the actuator saturation limits. In order to evaluate the structural adaptation algorithm, the following reference trajectory with high degree of maneuverability is considered:

$$\begin{cases} v_r(t) = -1.5 \sin(3t) \\ \omega_r(t) = \cos(2t - \pi/4) & \text{if } t < 3s \\ v_r(t) = -1.5 \\ \omega_r(t) = \sin(3t - \pi/4) & \text{if } 3s \leq t < 4.5s \\ v_r(t) = 1.5 \cos(0.5t) \\ \omega_r(t) = -\cos(2t - \pi/4) & \text{if } 4.5s \leq t \leq 8s \end{cases}$$

The reference trajectory initial posture is  $\mathbf{p}_r = (1.3, 0, \pi/2)$  and the mobile robot initial posture is  $\mathbf{p} = (1.15, 0, \pi/3)$ . The network weights are initialized randomly, with zero mean and standard deviation equal to 0.01. When a node is included into the structure, its weights are initialized in the same way. For performance comparison, two controllers are considered:

- Robust dynamic controller associated with the kinematic control – RK controller.
- Biased *wavelet* controller associated with the kinematic control – WK controller.

<sup>a</sup>  $\bar{\tau}_d$  is generated randomly, using a normal distribution with zero mean and standard deviation  $\sigma$ , i.e.,  $N(0; \sigma)$ .

The results are presented in figures 16–20.

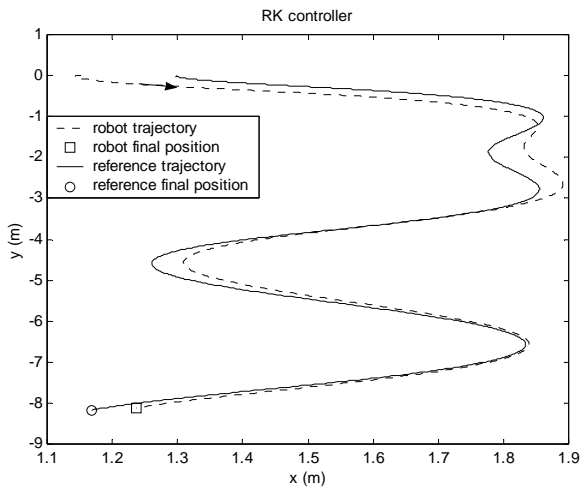


Figure 16: Robot and reference trajectory (RK controller)

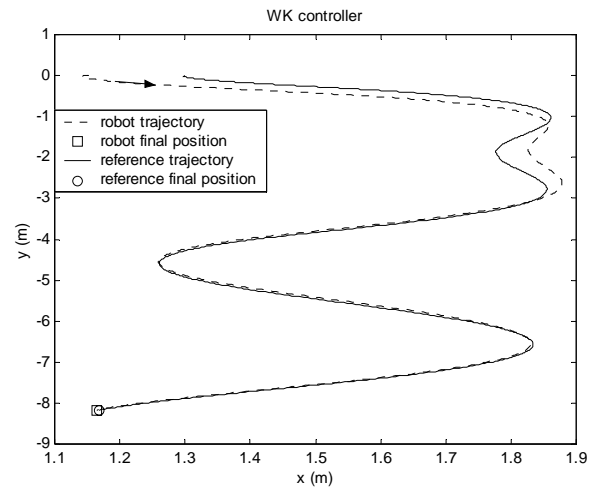


Figure 17: Robot and reference trajectory (WK controller)

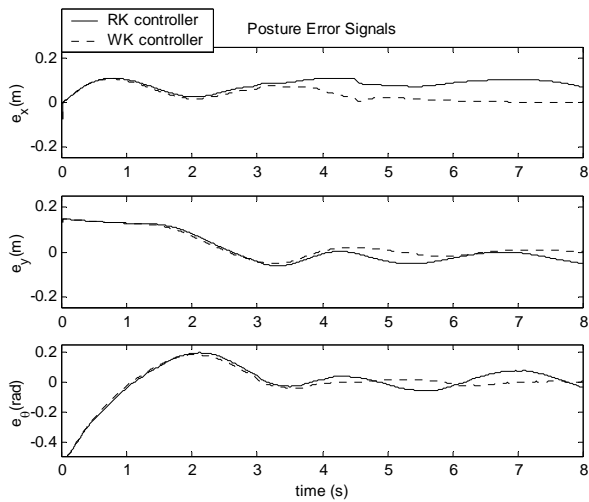


Figure 18: Posture error signals

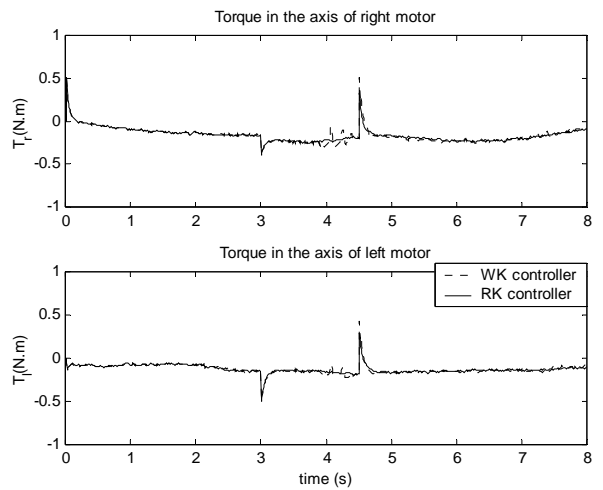


Figure 19: Torque in the right and left motors

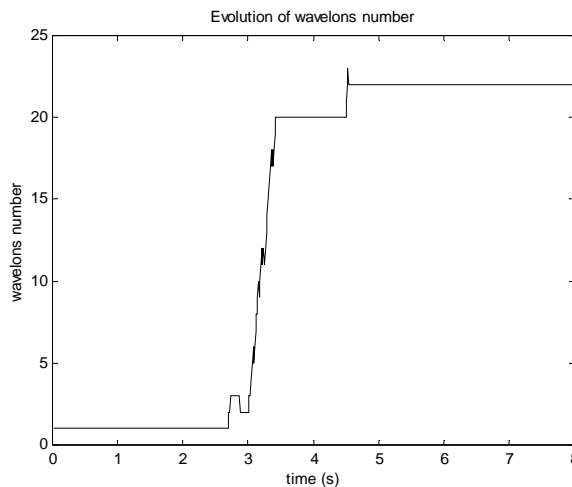


Figure 20: Evolution of wavelons number

Figures 16–18 show the performance improvement obtained by using the wavelet network in the dynamic controller, compensating the effect of surface friction and other disturbances. As we can see from figure 20, the BWN introduces new wavelons in the structure where the trajectory is fast changing, in order to improve the controller performance, as expected.

## 5.0 – CONCLUSIONS

In this work, a kinematic control law for mobile robots was proposed in cartesian coordinates, by using the frame system employed in [13]. The stability proof was based on a Lyapunov-like analysis. The proposed kinematic controller performance was evaluated via simulation and in real time by using the Magellan-ISR mobile robot. The results in real time were coherent with that obtained in simulation. The controller gains were adjusted experimentally, so as to provide smooth and fast transient response. The results obtained by the proposed kinematic controller can be considered satisfactory since the external perturbations and disturbances were not significant in real time implementation due to the fact that the robot trajectory was very smooth, such that the influence of the dynamic features in the controller performance could be neglected.

In order to improve the controller performance in the cases that the dynamic is significant, the proposed kinematic controller was augmented by a dynamic controller based on a biased wavelet network with structural adaptation. This aims at considering the dynamic effects and also the unmodeled dynamic, bounded disturbances and surface friction, which were all neglected in the kinematic model, described in Section 2. The simulations indicated the improvement obtained in dynamic controller performance by employing the wavelet network.

## 6.0 – ACKNOWLEDGEMENT

The authors thank to Atech, CCSIVAM and CNPQ–Pronex 662015/1998–3 for the support.

## 7.0 – REFERENCES

- [ 1] Y. Kanayama, Y. Kimura, F. Miyazaki and T. Noguchi: “A stable tracking control method for an autonomous mobile robot”, IEEE Int. Conf. on Robotics and Automation, 1990, Vol. 1, pp. 384-389.
- [ 2] C. J. Souza: “ Controle adaptativo de robôs móveis”, São José dos Campos: ITA, Msc Thesis, 2000.
- [ 3] M. Aicardi, G. Casalino, A. Bichhi and A. Balestrino: “ Closed loop steering of unicycle-like vehicles via Lyapunov techniques”, IEEE Robot. Automat. Mag., March 1995, Vol. 2, pp. 27-35.
- [ 4] R. Fierro and F. L. Lewis: “Control of a nonholonomic mobile robot using neural networks”, IEEE Trans. on Neural Networks, 1998, vol. 9, No. 4, pp. 589-600.
- [ 5] Q. Zhang: “ Using wavelet network in nonparametric estimation”, IEEE Trans. Neural Networks, March 1997, Vol. 8, pp. 227-236.
- [ 6] Q. Zhang and A. Benveniste: “ Wavelet network”, IEEE Trans. Neural Networks, November 1992, Vol. 3, pp. 889-898.
- [ 7] M. Cannon and J. J. E. Slotine: “ Space-frequency localized basis function networks for nonlinear system estimation and control”, Neurocomputing, 1995, Vol. 9, pp. 293-342.
- [ 8] Y. Yamamoto and X. Yun: “Coordinating locomotion and manipulation of a mobile manipulator”, IEEE Transactions on Automatic Control, 1994, Vol. 39, No. 6, pp. 1326-1332.
- [ 9] R. K. H. Galvão, T. Yoneyama and T. N. Rabello: “ Signal representation by adaptive biased wavelet expansions”, Digital Signal Process., October 1999, Vol. 9, No. 4, pp. 225-240.
- [10] R. M. Sanner and J. J. E. Slotine: “Structurally dynamic wavelet network for adaptive control of robotic systems”, Int. J. Contr., June 1998, Vol. 70, No 3, pp. 405-421.
- [11] G. Cybenko: “Approximation by superpositions of a sigmoidal function”, Mathematics of Control, Signals, and Systems, 1989, S. 1., Vol. 2, pp. 303-314.
- [12] IS Robotics: “ Magellan Pro Compact Mobile Robot User’s Guide”, 2000.
- [13] F. D. Del Rio: “ Analysis and evaluation of mobile robot control: application to electric wheelchairs”, Ph.D. University of Sevilla, Phd. Thesis, 1997.
- [14] A. V. J. Silveira and E. M. Hemerly: “Controle de robôs móveis em coordenadas retangulares via rede neural”, XIV Congresso Brasileiro de Automática, Anais, 2002, Natal-RN, pp.1266-1271.
- [15] A. V. J. Silveira and E. M. Hemerly: “ Controle de robôs móveis via rede wavelet”, Proceedings of the VI Brazilian Conference on Neural Networks, June 2003, pp. 67-72.
- [16] A. V. J. Silveira: “Controle cinemático e dinâmico de robôs móveis”, São José dos Campos:ITA, MSc Thesis, 2003.
- [17] J. J. E. Slotine and W. Li: “Applied nonlinear control”, New Jersey: Prentice Hall, 1991.
- [18] M. M. Polycarpou, M. J. Mears, and S. E. Weaver: “Adaptive wavelet control of nonlinear systems”, in Proc. IEEE Conf. Decision Contr., December 1997, pp. 3890-3895.